hybrid procedure probably impairs ventricular energetics compared to the Norwood procedure. However, it is very difficult to compare ventricular energetics among the different surgical procedures in the clinical settings because postoperative hemodynamic profiles, even heart rate and mean arterial pressure, are quite different among the palliations [12]. The lack of proper methodology to accurately measure hemodynamic parameters such as stroke volume in congenital heart diseases also limits the study in clinical settings. Therefore, to test the hypothesis that ventricular energetics are different among the palliations, we performed a theoretical analysis using computational models.

Materials and methods

We modeled the cardiovascular system for the hybrid procedure and that for the Norwood procedure using a systemic-to-pulmonary artery (SPA) shunt or a RV-PA shunt. The electrical analog of the hybrid procedure model used to simulate the cardiovascular system is shown in Fig. 1. Details of the Norwood procedure models with a SPA shunt and with a RV-PA shunt have been described previously [11]. Aortic and mitral atresias were assumed in all of the present models, and there was no left ventricle.

Heart

The ventricular and atrial chambers are represented by the time-varying elastance model [11, 13–15]. Pressure and volume of each chamber are related by

$$P_{cc}(t) = \left[P_{es,cc}(V_{cc}) - P_{ed,cc}(V_{cc})\right] e_{cc}(t) + P_{ed,cc}(V_{cc}) \quad (1)$$

$$P_{ed,cc} = A_{cc}\left[e^{B_{cc}(V_{ed,cc}-V_{0,cc})} - 1\right] \quad (2)$$

$$P_{es,cc} = E_{es,cc}[V_{es,cc} - V_{0,cc}] \quad (3)$$

$$e_{cc}(t) = 0.5[1 - \cos(\pi t/T_{es,cc})] \quad (0 \le t < 2T_{es,cc})$$

$$e_{cc}(t) = 0 \quad (2T_{es,cc} \le t < T_c), \quad (4)$$

where P_{cc} and V_{cc} are pressure and volume, respectively, of each chamber [cc denotes the right atrial (RA), left atrial (LA), or right ventricular (RV) chamber], and t is the time from the start of systole. We modeled chamber pressure as the sum of end-diastolic pressure ($P_{ed,\,cc}$, Eq. 2) and the developed pressure [difference between end-systolic ($P_{es,\,cc}$, Eq. 3) and $P_{ed,\,cc}$] scaled by normalized elastance [$e_{cc}(t)$, Eq. 4]. Other parameters are listed in Table 1 [11, 13–16]. The time advance of atrial systole (DT) is calculated as $DT = 0.02T_c$ [11, 16].

Restrictive atrial septal defect (R_{ASD}) is described as a constant resistance, and the value in the hybrid procedure model was set 10 times higher than those of the Norwood procedure models. Each valve is represented as an ideal diode connected serially to a small resistor (pulmonary, R_{PV}; tricuspid, R_{TV}).

Vascular system

Pulmonary and systemic circulations are modeled as modified Windkessel models. Each vasculature is modeled by lumped venous (C_v) and arterial (C_a) capacitances, a characteristic impedance (R_c), arterial resistance (R_a), and a resistance proximal to C_v (R_v). Linear relation between pressure drop and flow in each resistance (except for PA banding), relation

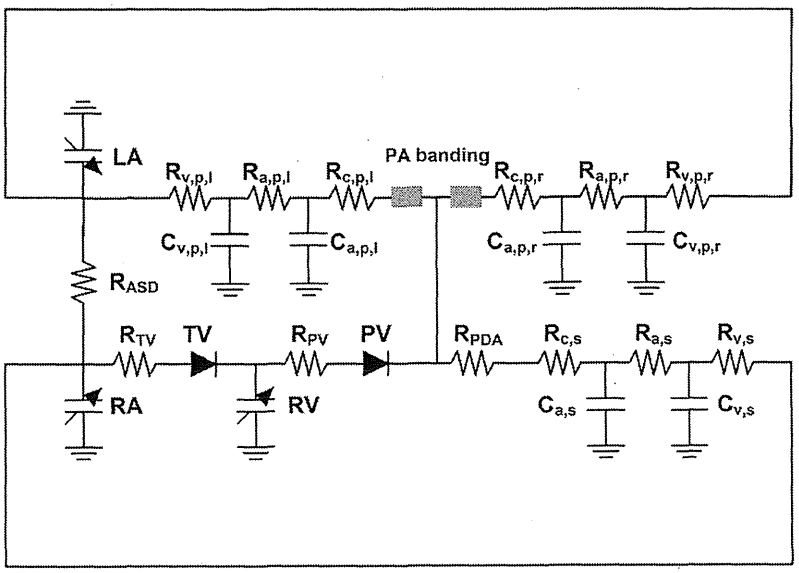

Fig. 1 Electrical analog of the hybrid procedure. *LA* left atrium, *RA* right atrium, *RV* right ventricle, *PV* pulmonary valve, *TV* tricuspid valve, *ASD* atrial septal defect, *PDA* patent ductus arteriosus, R_a arterial resistance, R_c characteristic impedance, R_v venous resistance, C_a arterial capacitance, C_v venous capacitance. *s* and *p* denote systemic and pulmonary circulation, respectively. *l* and *r* denote *left* and *right* sides, respectively. R_{PV}, R_{TV}, R_{ASD} and R_{PDA} represent resistance at PV, TV, ASD and PDA, respectively

Table 1 Parameters used in modeling of hybrid procedure

Heart rate (HR) (beats/min)			150
Duration of cardiac cycle (T_c) (ms)			400
	RV	RA	LA
Time to end systole (T_{es}) (ms)	140	60	60
End-systolic elastance (E_{es}) (mmHg/ml)	8.5	7.35	7.35
Scaling factor of EDPVR (A) (mmHg)	*0.9*	*0.17*	*0.17*
Exponent for EDPVR (B) (ml^{-1})	0.062	0.484	0.484
Unstressed volume (V_0) (ml)	4	1	1
	Pulmonary		Tricuspid
Valvular resistance (forward) (mmHg s ml^{-1})	0.0004		0.00004
Resistance (mmHg s ml^{-1})	ASD		
	0.01		
Resistance (mmHg s ml^{-1})	PDA		
	0.0004		
	PA banding		
Diameter of proximal PA (D_{PA}) (mm)	5.0		
Constant (k) (mmHg $(l/s)^{-2}$ mm^4)	1.62×10^6		
	Systemic (s)	Pulmonary (p)	
		Lt. (l)	Rt. (r)
Arterial resistance (R_a) (mmHg s ml^{-1})	3.83	1.56	1.04
Characteristic impedance (R_c) (mmHg s ml^{-1})	0.20	0.071	0.047
Venous resistance (R_v) (mmHg s ml^{-1})	0.083	0.027	0.018
Arterial capacitance (C_a) (ml/mmHg)	0.50	0.13	0.19
Venous capacitance (C_v) (ml/mmHg)	4.39	0.36	0.53

RV right ventricle, *RA* right atrium, *LA* left atrium, *EDPVR* end-diastolic pressure–volume relation, *ASD* atrial septal defect, *PDA* patent ductus arteriosus, *PA* pulmonary artery, *Lt* left, *Rt* right

between pressure (P_c) and volume (V_c) in each capacitance C (Eq. 5), and the change in volume in each capacitance [$dV(t)/dt$] calculated by the difference between inflow and outflow (Eq. 6) are used to describe each vasculature:

$$P_c = \frac{V_c}{C} \tag{5}$$

$$\frac{dV(t)}{dt} = \sum Q_{inflow}(t) - \sum Q_{outflow}(t) \tag{6}$$

where $Q_{inflow}(t)$ and $Q_{outflow}$ (t) are volumetric inflow and outflow, respectively.

Ideal ductal stenting without stenosis (R_{PDA}) is described as a constant resistance.

Pressure drop across the PA banding

Combining the Bernoulli's principle, the relation between PA flow velocity V (V_{PAB}, banding site; V_{PA}, PA proximal to the banding site), volumetric flow of the right or left PA $Q(t)$, and PA diameter D (D_{PAB}, banding site; D_{PA}, proximal PA) are represented as follows:

$$\Delta P(t) = \frac{1}{2}\rho\left(V_{PAB}^2 - V_{PA}^2\right), \quad V_{PAB} = \frac{4Q(t)}{\pi D_{PAB}^2}, \quad V_{PA} = \frac{4Q(t)}{\pi D_{PA}^2}$$

And, pressure drop across the PA banding [$\Delta P(t)$] is described as

$$\Delta P(t) = k\left(\frac{1}{D_{PAB}^4} - \frac{1}{D_{PA}^4}\right)Q(t)^2, \quad k = \frac{8\rho}{\pi^2}, \tag{7}$$

where ρ is blood density ($\rho = 1.06$ g/cm^3), and k is constant if the blood density does not change.

Protocols

First, the control state was simulated using the 4.0-mm SPA shunt Norwood procedure model. Total stressed blood volume (V_s), which is the sum of the stressed volumes in all capacitances and in all chambers, was set as 81.4 ml.

$$Vs = V_{RV} + V_{LA} + V_{RA} + V_{Ca,s} + V_{Cv,s} + V_{Ca,p,l} + V_{Cv,p,l} + V_{Ca,p,r} + V_{Cv,p,r} \quad (8)$$

We solved the simultaneous differential equations (Eqs. 1–8) using MATLAB/Simulink (MathWorks, Inc., MA, USA).

Shunt diameter was decreased stepwise from 4.0 to 3.0 mm in decrements of 0.5 mm in the original Norwood procedure model using a SPA shunt, and increased from 4.0 mm to 6.0 mm at increments of 1.0 mm in the modified Norwood procedure model using a RV-PA shunt. Diameter of the PA banding was increased from 1.5 to 2.0 mm in increments of 0.25 mm in the hybrid procedure model. Systemic and pulmonary flow (Q_s and Q_p), systemic and pulmonary arterial pressures (SAP and PAP), systemic-to-pulmonary diastolic run-off or diastolic regurgitation from PA to RV, right ventricular end-diastolic volume (RVEDV), stroke work (SW), systolic pressure–volume area (PVA), and mechanical efficiency (SW/PVA) after each procedure were calculated for each shunt or banding diameter. Heart rate and SAP widely vary in clinical settings. This makes it difficult to compare the procedural effects. Therefore, to provide a proper comparison among the three different procedures, heart rate was fixed at 150 bpm and mean SAP was set at the same value as that of the control state, by adjusting the total stressed blood volume (V_s).

Calculation of arterial and venous oxygen saturation

Arterial (SaO_2) and venous O_2 saturation (SvO_2) are calculated by the following equations for Q_p and Q_s (l/min):

$$SaO_2 = S_{PV}O_2 - \frac{CVO_2 \times BSA}{1.34 \times Hb \times 10 \times Q_p}$$

$$SvO_2 = SaO_2 - \frac{CVO_2 \times BSA}{1.34 \times Hb \times 10 \times Q_s}$$

where $S_{PV}O_2$ is the pulmonary venous O_2 saturation (0.97), CVO_2 is the whole body O_2 consumption (185 ml O_2/min/m^2), BSA is the body surface area (0.20 m^2), Hb is the hemoglobin concentration (16.0 g/dl), and 10 (dl/l) and 1.34 (ml O_2/g) are conversion factors [11, 16, 17].

Results

By adjusting the stressed blood volume, mean SAP and Q_s were maintained at around 58.7 mmHg and 0.83 l/min, respectively, in all the models.

In the hybrid procedure model, looser PA banding increased systolic SAP and decreased diastolic SAP. In the SPA shunt Norwood procedure model, systolic SAP increased and diastolic SAP decreased with the use of a larger shunt. In the RV-PA shunt Norwood procedure model, however, change in shunt diameter affected systolic and diastolic SAP only slightly (Fig. 2a). In all the models, mean PAP (Fig. 2b), Q_p (Fig. 2c) and Q_p/Q_s (Fig. 2d) increased with increase in diameter. These parameters were almost equivalent among the 1.75-mm hybrid procedure (13.7 mmHg, 0.97 l/min and 1.18, respectively), 3.5-mm SPA shunt (13.9 mmHg, 1.04 l/min and 1.27), and 6.0-mm RV-PA shunt (11.6 mmHg, 0.86 l/min and 1.05) models. The SaO_2 and SvO_2 also were elevated with increase in diameter (Fig. 2e). The SaO_2 and SvO_2 were almost equivalent among the 1.75-mm hybrid procedure (79.2 and 58.1 %, respectively), 3.5-mm SPA shunt (80.4 and 59.4 %), and 6.0-mm RV-PA shunt (77.0 and 56.1 %) models. Use of a larger caliber conduit in the SPA shunt Norwood procedure and a looser band in the hybrid procedure caused a significant increase in diastolic run-off from systemic to pulmonary circulation. Use of a larger caliber conduit in the RV-PA shunt Norwood procedure also caused an increase in diastolic regurgitation from PA to RV, but this increase was smaller than those in diastolic run-off (Fig. 2f).

The pressure–volume loops of the 1.75-mm hybrid procedure as well as the 3.5-mm SPA shunt and 6.0-mm RV-PA shunt Norwood procedures are shown in Fig. 3. Although RVEDV did not differ among the 1.75-mm hybrid procedure (23.6 ml), 3.5-mm SPA shunt (24.1 ml), and 6.0-mm RV-PA shunt (23.0 ml) (Fig. 4a), SW was slightly smaller in the 6.0-mm RV-PA shunt (873 mmHg ml) than in the 1.75-mm hybrid procedure (929 mmHg ml) or the 3.5-mm SPA shunt (974 mmHg ml) (Fig. 4b). Furthermore, systolic PVA in the 6.0-mm RV-PA shunt (992 mmHg ml) was significantly smaller than that in the 1.75-mm hybrid procedure (1,184 mmHg ml) or the 3.5-mm SPA shunt (1,228 mmHg ml) (Fig. 4c). As a result, mechanical efficiency (SW/PVA) was higher in the 6.0-mm RV-PA shunt (88.0 %) than in the 1.75-mm hybrid procedure (78.5 %) or the 3.5-mm SPA shunt (79.3 %) (Fig. 4d). The relation between Q_p/Q_s and mechanical efficiency was almost superimposed for the hybrid procedure and the SPA shunt Norwood procedure, but efficiency was much better in the RV-PA shunt Norwood procedure at all Q_p/Q_s levels (Fig. 5).

Discussion

Advantages of hybrid procedure

The present computational study revealed that the hemodynamics provided by the hybrid procedure is comparable to that by the conventional Norwood procedure using a SPA shunt, but is less favorable than that by the modified

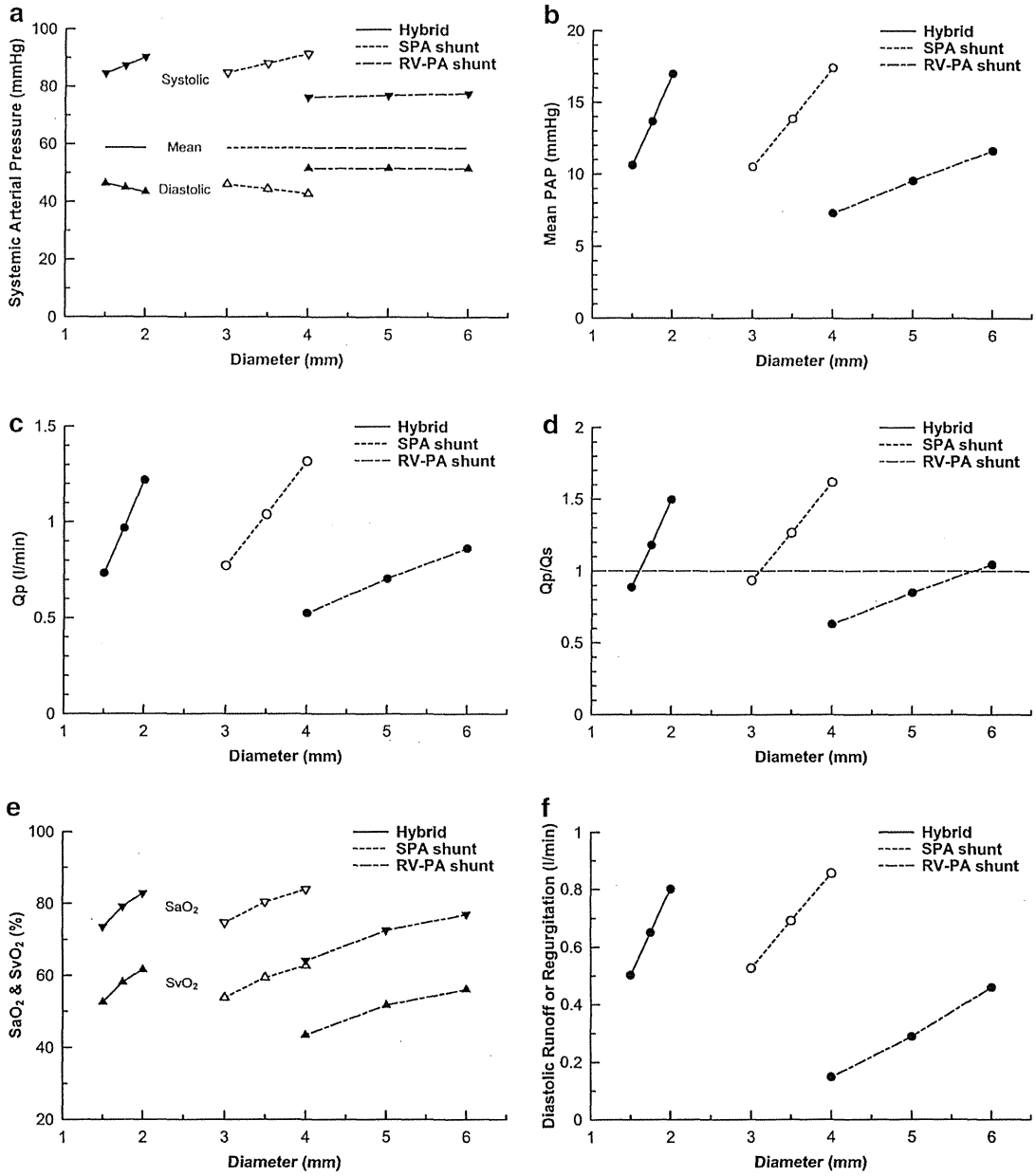

Fig. 2 The relations between shunt or banding diameter and systemic arterial pressure (**a**), mean pulmonary artery pressure (PAP, **b**), pulmonary flow (Q_p, **c**), ratio of pulmonary to systemic flow (Q_p/Q_s, **d**), arterial and venous saturation (SaO_2 and SvO_2, respectively, **e**) and diastolic run-off or regurgitation (**f**). Mean PAP was the average of the *left* and *right* mean PAP and Q_p was the sum of the *left* and *right* pulmonary flow in the hybrid procedure model. *Solid line*, hybrid procedure; *dotted line*, systemic to pulmonary artery (SPA) shunt; *dot-dashed line*, right ventricle to pulmonary artery (RV-PA) shunt

Norwood procedure using a RV-PA shunt. The 1.75-mm hybrid procedure was almost equivalent to the 3.5-mm SPA shunt Norwood procedure from the viewpoint of postoperative hemodynamics. Therefore, without using CPB, the hybrid procedure may be able to achieve similar clinical outcome as the SPA shunt Norwood procedure even in high-risk patients.

In low-weight infants, the Norwood procedure and its modification are a risk factor for increased mortality. Several studies have reported that infants weighing less than 2.5 kg have a significantly higher mortality after the Norwood procedure [18, 19]. The CPB procedure per se is unlikely to be a risk factor associated with early postoperative mortality due to recent improvements in cardiovascular

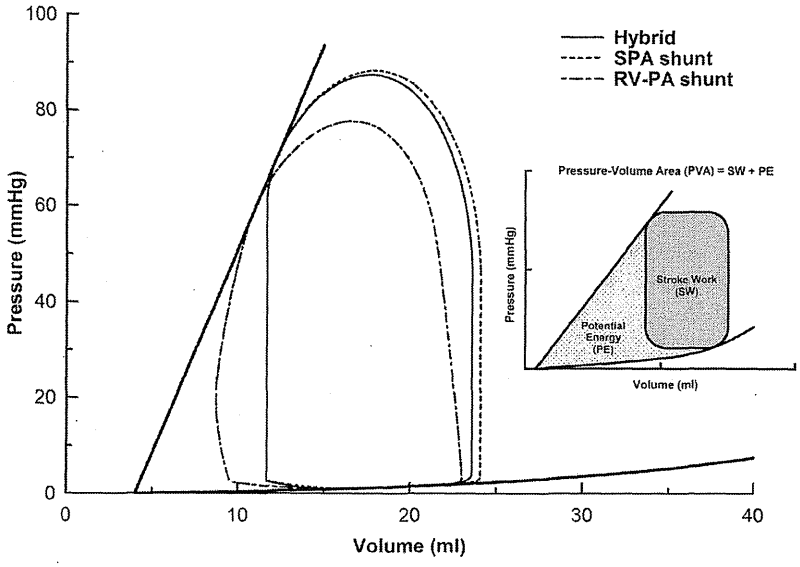

Fig. 3 Simulated pressure–volume loops of the 1.75-mm hybrid procedure (*solid line*), the Norwood procedure with a 3.5-mm systemic to pulmonary artery (SPA) shunt (*dotted line*) and Norwood procedure with a 6.0-mm right ventricle to pulmonary artery (RV-PA) shunt (*dot-dashed line*)

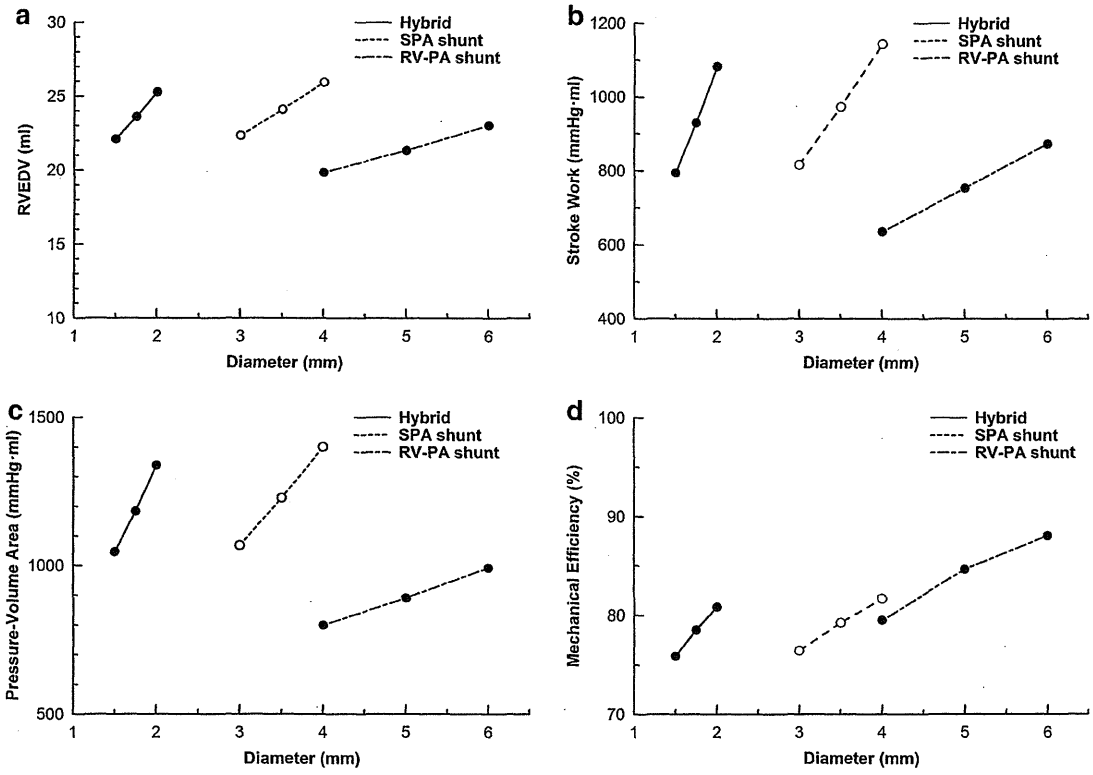

Fig. 4 The relations between shunt or banding diameter and right ventricular end-diastolic volume (RVEDV, **a**), stroke work (**b**), systolic pressure–volume area (**c**) and mechanical efficiency (**d**). *Solid line*, hybrid procedure; *dotted line*, systemic to pulmonary artery (SPA) shunt; *dot-dashed line*, right ventricle to pulmonary artery (RV-PA) shunt

management during CPB [20]. However, Pawade et al. [21] reported that the risk factors associated with an increased risk of early death in infants weighing less than 2.5 kg undergoing reconstruction surgery using CPB were (1) presence of preoperative metabolic acidosis; (2) univentricular repair; and (3) duration of cardiopulmonary bypass.

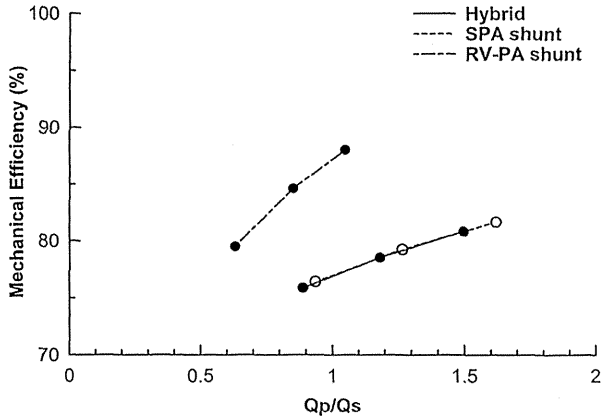

Fig. 5 The relation between Q_p/Q_s and mechanical efficiency. *Solid line*, hybrid procedure; *dotted line*, systemic to pulmonary artery (SPA) shunt; *dot-dashed line*, right ventricle to pulmonary artery (RV-PA) shunt

Weinstein et al. [22] also reported a trend toward increased mortality with increased CPB time in HLHS infants weighting less than 2.5 kg. Since the hybrid procedure does not require CPB, increased CPB time is not a concern. Pizarro et al. [23] have reported that patients undergoing hybrid palliation have lower preoperative blood pH than Norwood patients. This may reflect the surgeons' selection of hybrid procedure for high-risk infants. In their study, there were no significant differences in hospital and interstage mortalities between the hybrid and the conventional Norwood strategies. Because preoperative metabolic acidosis is associated with increased risk of early death after CPB [21], the most suitable patients for the hybrid procedure may be low-weight infants with preoperative metabolic acidosis.

Disadvantages of hybrid procedure

The hybrid procedure is very sensitive to a change in diameter of the banding site. A slight increase in diameter readily causes pulmonary over-circulation. In the present study, an increase in diameter of only 0.25 mm (from 1.75 to 2.0 mm) resulted in a 26.0 % increase in Q_p (Fig. 2c). Thus, surgeons have to adjust the band size carefully to avoid pulmonary over-circulation or malperfusion.

The present study provides important insight into ventricular energetics of the hybrid procedure. The hybrid procedure cannot reduce PVA while the Norwood procedure with RV-PA shunt can reduce PVA. The PVA in the 1.75-mm hybrid procedure was 19.3 % larger than that in the 6.0-mm RV-PA shunt Norwood procedure. Thus, the hybrid procedure maintains systemic circulation at the expense of higher oxygen consumption compared to the RV-PA shunt. Because coronary blood flow depends on myocardial oxygen demand under physiological conditions [24], the hybrid procedure requires more coronary blood flow than the RV-PA shunt to maintain the same systemic circulation. This feature may impair coronary flow reserve. The hybrid procedure may have poor tolerance to postoperative myocardial oxygen supply/demand imbalance.

The hybrid procedure as well as the SPA shunt Norwood procedure cannot avoid diastolic run-off from the systemic to pulmonary circulation. Therefore, the hybrid procedure requires more stressed blood volume to maintain systemic cardiac output (Q_s) at the same level as the Norwood procedure with the RV-PA shunt. This means that the hybrid procedure may easily cause volume overload to the single ventricle. In addition, the present study demonstrates that mechanical efficiency in the 1.75-mm hybrid procedure is 9.5 % lower compared to the 6.0-mm RV-PA shunt. Using the hybrid procedure, the RV must pump blood to a high-pressure system, i.e., the systemic circulation. Thereafter, a portion of the blood flows into a low pressure system, i.e., the pulmonary circulation, according to the pressure gradient. Using the RV-PA shunt, however, RV can simultaneously eject blood to both high- and low-pressure systems. This difference in mechanics results in increased elastic potential energy (Fig. 3) and reduced mechanical efficiency (SW/PVA) for the hybrid procedure compared to the RV-PA shunt. The impaired mechanical efficiency may be associated with the clinical observation that the hybrid procedure does not improve interstage mortality although this approach reduces the initial surgical insult [23].

Limitations

First, intraoperative use of cardiopulmonary bypass and circulatory arrest in the Norwood procedure may affect the postoperative ventricular performance. Furthermore, the right ventriculotomy in the Norwood procedure with the RV-PA shunt may impair ventricular contractility. These factors may reduce potential advantage on ventricular energetics of the Norwood procedure compared with the hybrid procedure. However, our previous simulation study has indicated the Norwood procedure with the RV-PA shunt still has an advantage on ventricular energetics even when end-systolic elastance is reduced by approximately 20 % [11].

Second, in the present study, mean arterial pressure and Q_s were fixed for all of the models, and the results need to be interpreted accordingly. In other words, actual ventricular performance could depend on a given hemodynamic state in each patient.

Third, a patient-specific simulation may be helpful to understand the patient's fluid dynamics [25]. However, our present model was based on the previous studies [11, 13–16] and not a patient-specific model. To perform a

patient-specific simulation, we have to develop an accurate method of estimating the parameters for simulation, such as elastance, resistance and compliance.

Conclusions

Although the hybrid procedure has the advantage of requiring no CPB, this procedure provides similar hemodynamics as the conventional Norwood procedure using a SPA shunt and has greater myocardial oxygen demand compared to the modified Norwood procedure using a RV-PA shunt.

Acknowledgments The present study was supported by a research project promoted by the Japanese Ministry of Health, Labour and Welfare (H20-katsudo-Shitei-007) and Grants-in-Aid for Scientific Research (No. 22791328) from the Ministry of Education, Culture, Sports, Science and Technology.

Conflict of interest The authors declare that they have no conflict of interest.

Ethical standards Because this study is a simulation study, the declaration about ethics does not apply to this study.

References

1. Gibbs JL, Wren C, Watterson KG, Hunter S, Hamilton JR (1993) Stenting of the arterial duct combined with banding of the pulmonary arteries and atrial septectomy or septostomy: a new approach to palliation for the hypoplastic left heart syndrome. Br Heart J 69:551–555
2. Venugopal PS, Luna KP, Anderson DR, Austin CB, Rosenthal E, Krasemann T, Qureshi SA (2010) Hybrid procedure as an alternative to surgical palliation of high-risk infants with hypoplastic left heart syndrome and its variants. J Thorac Cardiovasc Surg 139:1211–1215
3. Caldarone CA, Benson L, Holtby H, Li J, Redington AN, Van Arsdell GS (2007) Initial experience with hybrid palliation for neonates with single-ventricle physiology. Ann Thorac Surg 84:1294–1300
4. Galantowicz M, Cheatham JP, Phillips A, Cua CL, Hoffman TM, Hill SL, Rodeman R (2008) Hybrid approach for hypoplastic left heart syndrome: intermediate results after the learning curve. Ann Thorac Surg 85:2063–2070
5. Photiadis J, Sinzobahamvya N, Hraška V, Asfour B (2012) Does bilateral pulmonary banding in comparison to Norwood procedure improve outcome in neonates with hypoplastic left heart syndrome beyond second-stage palliation? A review of the current literature. Thorac Cardiovasc Surg 60:181–188
6. Sasaki T, Takahashi Y, Ando M, Wada N, Kawase Y, Seki H (2008) Bilateral pulmonary artery banding for hypoplastic left heart syndrome and related anomalies. General Thorac Cardiovasc Surg 56:158–162
7. Sano S, Ishino K, Kawada M, Arai S, Kasahara S, Asai T, Masuda Z, Takeuchi M, Ohtsuki S (2003) Right ventricle-pulmonary artery shunt in first-stage palliation of hypoplastic left heart syndrome. J Thorac Cardiovasc Surg 126:504–509
8. Sharma V, Deo SV, Huebner M, Dearani JA, Burkhart HM (2014) In search of the ideal pulmonary blood source for the Norwood procedure: a meta-analysis and systematic review. Ann Thorac Surg 98:142–150
9. Lee N, Das A, Banerjee RK, Gottliebson WM (2013) Comparison of stroke work between repaired tetralogy of Fallot and normal right ventricular physiologies. Heart Vessels 28:76–85
10. Bove EL, Migliavacca F, de Leval MR, Balossino R, Pennati G, Lloyd TR, Khambadkone S, Hsia TY, Dubini G (2008) Use of mathematic modeling to compare and predict hemodynamic effects of the modified Blalock–Taussig and right ventricle-pulmonary artery shunts for hypoplastic left heart syndrome. J Thorac Cardiovasc Surg 136:312–320
11. Shimizu S, Une D, Shishido T, Kamiya A, Kawada T, Sano S, Sugimachi M (2011) Norwood procedure with non-valved right ventricle to pulmonary artery shunt improves ventricular energetics despite the presence of diastolic regurgitation: a theoretical analysis. J Physiol Sci 61:457–465
12. Li J, Zhang G, Benson L, Holtby H, Cai S, Humpl T, Van Arsdell GS, Redington AN, Caldarone CA (2007) Comparison of the profiles of postoperative systemic hemodynamics and oxygen transport in neonates after the hybrid or the Norwood procedure: a pilot study. Circulation 116(Suppl):I179–I187
13. Burkhoff D, Tyberg JV (1993) Why does pulmonary venous pressure rise after onset of LV dysfunction: a theoretical analysis. Am J Physiol 265:H1819–H1828
14. Morley D, Litwak K, Ferber P, Spence P, Dowling R, Meyns B, Griffith B, Burkhoff D (2007) Hemodynamic effects of partial ventricular support in chronic heart failure: results of simulation validated with in vivo data. J Thorac Cardiovasc Surg 133:21–28
15. Shimizu S, Shishido T, Une D, Kamiya A, Kawada T, Sano S, Sugimachi M (2010) Right ventricular stiffness constant as a predictor of postoperative hemodynamics in patients with hypoplastic right ventricle: a theoretical analysis. J Physiol Sci 60:205–212
16. Migliavacca F, Pennati G, Dubini G, Fumero R, Pietrabissa R, Urcelay G, Bove EL, Hsia TY, de Leval MR (2001) Modeling of the Norwood circulation: effects of shunt size, vascular resistances, and heart rate. Am J Physiol Heart Circ Physiol 280:H2076–H2086
17. Chang AC, Kulik TJ, Hickey PR, Wessel DL (1993) Real-time gas-exchange measurement of oxygen consumption in neonates and infants after cardiac surgery. Crit Care Med 21:1369–1375
18. Curzon CL, Milford-Beland S, Li JS, O'Brien SM, Jacobs JP, Jacobs ML, Welke KF, Lodge AJ, Peterson ED, Jaggers J (2008) Cardiac surgery in infants with low birth weight is associated with increased mortality: analysis of the Society of Thoracic Surgeons Congenital Heart Database. J Thorac Cardiovasc Surg 135:546–551
19. Sano S, Huang SC, Kasahara S, Yoshizumi K, Kotani Y, Ishino K (2009) Risk factors for mortality after the Norwood procedure using right ventricle to pulmonary artery shunt. Ann Thorac Surg 87:178–185
20. Shepard CW, Kochilas LK, Rosengart RM, Brearley AM, Bryant R 3rd, Moller JH, St Louis JD (2010) Repair of major congenital cardiac defects in low-birth-weight infants: is delay warranted? J Thorac Cardiovasc Surg 140:1104–1109
21. Pawade A, Waterson K, Laussen P, Karl TR, Mee RB (1993) Cardiopulmonary bypass in neonates weighing less than 2.5 kg: analysis of the risk factors for early and late mortality. J Card Surg 8:1–8
22. Weinstein S, Gaynor JW, Bridges ND, Wernovsky G, Montenegro LM, Godinez RI, Spray TL (1999) Early survival of infants weighing 2.5 kilograms or less undergoing first-stage reconstruction for hypoplastic left heart syndrome. Circulation 100(Suppl):II167–II170
23. Pizarro C, Derby CD, Baffa JM, Murdison KA, Radtke WA (2008) Improving the outcome of high-risk neonates with

hypoplastic left heart syndrome: hybrid procedure or conventional surgical palliation? Eur J Cardiothorac Surg 33:613–618
24. Tune JD, Gorman MW, Feigl EO (2004) Matching coronary blood flow to myocardial oxygen consumption. J Appl Physiol 97:404–415
25. Sughimoto K, Takahara Y, Mogi K, Yamazaki K, Tsubota K, Liang F, Liu H (2014) Blood flow dynamic improvement with aneurysm repair detected by a patient-specific model of multiple aortic aneurysms. Heart Vessels 29:404–412

frontiers in PHYSIOLOGY

PERSPECTIVE ARTICLE
published: 08 July 2014
doi: 10.3389/fphys.2014.00256

Systems physiology of the baroreflex during orthostatic stress: from animals to humans

Atsunori Kamiya *, Toru Kawada and Masaru Sugimachi

Department of Cardiovascular Dynamics, National Cerebral and Cardiovascular Center Research Institute, Suita, Japan

Edited by:
Qi Fu, The Institute for Exercise and Environmental Medicine and University of Texas Southwestern Medical Center, USA

Reviewed by:
Vaughan G. Macefield, University of Western Sydney, Australia
J. A. Taylor, Harvard University, USA

****Correspondence:***
Atsunori Kamiya, Department of Cardiovascular Dynamics, National Cerebral and Cardiovascular Center Research Institute, 5-7-1 Fujishirodai, Suita, Osaka 565-8565, Japan
e-mail: kamiya@ri.ncvc.go.jp

The baroreflex is a key mechanism involved in the control of arterial pressure (AP) during orthostasis in humans. However, the baroreflex is a closed-loop feedback system, from baroreceptor pressure input to systemic AP, and therefore requires open-loop experiments to identify its system characteristics. The requirement limits our ability to identify baroreflex system characteristics in humans. Open-loop research in animals has revealed dynamic and static characteristics of the two baroreflex subsystems: the neural and peripheral arcs. The neural arc, from baroreceptor pressure input to sympathetic nerve activity (SNA), has high-pass dynamic characteristics, indicating that more rapid change in input AP causes greater response in SNA. In contrast, the peripheral arc, from SNA input to systemic AP, has low-pass characteristics. Orthostasis increases the gain of the neural arc, which compensates for the lower transfer gain of the peripheral arc and in turn maintains total baroreflex function. Here, I discuss the possibility that baroreflex subsystem characteristics identified in animals can be applicable to the human sympathetic response to orthostasis, with a focus on loading speed-dependence of orthostatic sympathetic activation.

Keywords: baroreflexes, systems analysis, sympathetic nerve activity, autonomic nervous system, integrative physiology

INTRODUCTION

The maintenance of arterial pressure (AP) under orthostatic stress from gravitational fluid shift is of great importance in humans (Eckberg and Sleight, 1992) and animals (rats, rabbits etc.) that spend most of their time in a head-up posture and that frequently stand during their daily life. The baroreflex is a key mechanism involved in the control of AP during orthostasis since baroreflex failure leads to severe orthostatic hypotension (Cooke et al., 1999; Fu et al., 2009). The baroreflex is a negative-feedback closed-loop system, from baroreceptor pressure input to systemic AP, and therefore needs open-loop surgical operation to identify its system characteristics (Ikeda et al., 1996), which is fundamentally impossible in human research. Animal research that has used open-loop baroreflex and white-noise input techniques (system identification) have clarified dynamic and static transfer characteristics of the two baroreflex subsystems, the neural arc and peripheral arc, during orthostasis as described below.

Regarding the dynamic transfer characteristics, the neural arc, from baroreceptor pressure input to SNA, has high-pass dynamic characteristics, which means that a more rapid change in AP results in a greater response in SNA, whereas the peripheral arc, from SNA input to systemic AP, has low-pass dynamic characteristics (Kawada et al., 2002; Kamiya et al., 2005c). The open-loop transfer function of the neural arc is able to predict time-series SNA responses to drug-induced AP changes with an r^2 of 0.9, whereas the closed-loop-spontaneous transfer function cannot with a negative r-value (the inverse of measured responses) (Kamiya et al., 2011). In addition, orthostatic stress, caused from movement from a horizontally supine position, increases the transfer function gain of the neural arc, which helps compensate for the lower transfer function gains of the peripheral arc during orthostasis. This in turn helps maintain total baroreflex function (Kamiya et al., 2008). Regarding the static transfer characteristics, orthostatic stress resets the neural arc (baroreceptor pressure-SNA curve) to a higher SNA level (in the kidney and the heart), which compensates for the reduced presser responses to an increase in SNA in the peripheral cardiovascular system and helps prevent postural hypotension (Kamiya et al., 2005b, 2010).

Although system identification of the baroreflex is a useful tool for understanding baroreflex function in a variety of physiological and pathophysiological conditions, it requires surgical operation to open the baroreflex loop. The requirement of an open-loop experimental condition limits its application in human research. Therefore, the system characteristics of the baroreflex identified in animals, particularly the dynamic transfer function characteristics, have not been related to human baroreflex physiology.

Here, I discuss the possibility that baroreflex subsystem characteristics identified in animals can be applicable to the human sympathetic response to orthostasis. I will focus on the high-pass filter dynamic transfer function characteristics identified in muscle, cardiac and renal SNA of anesthetized rabbits (Kamiya et al., 2005c). I will also discuss whether transfer function characteristics identified in animals can explain the previously reported finding in humans that slow head-up tilt causes lower activation of muscle SNA (MSNA): loading speed-dependence of orthostatic sympathetic activation in humans (Kamiya et al., 2009).

SPEED-DEPENDENCE OF ORTHOSTATIC SYMPATHETIC ACTIVATION IN HUMANS

A stronger orthostatic stress causes greater MSNA response during head-up tilt (HUT) and thus it is well known that orthostatic MSNA activation is amplitude-dependent (Eckberg and Sleight, 1992; Cooke et al., 1999; Fu et al., 2009). In contrast, less attention has been paid to the effects of loading speed of orthostatic stress on orthostatic sympathetic activation in humans. Our previous study (Kamiya et al., 2009) examined whether the inclining speed of HUT influences the MSNA response to passive 30° HUT, independent of the magnitude of HUT, using inclining speeds of 1, 0.1, and 0.0167°/s (RAPID, SLOW, and VERYSLOW tests, respectively), in 12 healthy subjects (**Figure 1**). Calf MSNA (averaged over every 10° tilt angle) increased during inclination from 0 to 30°, with greater increases in the RAPID test than SLOW and VERYSLOW tests. In addition, only the RAPID test caused MSNA overshoot after reaching 30° HUT, whereas the SLOW and VERYSLOW tests did not. These results indicate that slower HUT results in smaller activation of MSNA suggesting that HUT-induced sympathetic activation depends partially on the speed of inclination during HUT in humans. The speed-dependence was also found in the high frequency amplitude of R-R interval variability (an index of cardiac vagal nerve activity), that decreased to a lesser extent during the inclination and after reaching 30° in the VERYSLOW test compared to the RAPID test.

CHARACTERISTICS OF BAROREFLEX SUBSYSTEMS IN ANIMALS: NEURAL AND PERIPHERAL ARCS

Previous system identification using open-loop experiments and transfer function analysis, commonly used in engineering, have revealed that in anesthetized animals (for example, rabbits), the transfer function of the neural arc (baroreceptor pressure to SNA) approximates derivative characteristics in the frequency range below 0.8 Hz, and high-cut characteristics of frequencies above 0.8 Hz (Kamiya et al., 2005c).Therefore, the neural arc transfer function (H_N) can be modeled by using Equation A as follows:

$$H_N(f) = -K_N \frac{1 + \frac{f}{fc1}j}{\left(1 + \frac{f}{fc2}\right)^2} \exp(-2\pi fjL) \qquad (A)$$

where f and j represent the frequency (in Hz) and imaginary units, respectively; K_N is static gain (in a.u./mmHg); $fc1$ and $fc2$ ($fc_1 < fc_2$) are corner frequencies (in Hz) for derivative and high-cut characteristics, respectively; and L is pure delay (in seconds), that would represent the sum of delays in the synaptic transmission at the baroreflex central pathways and the sympathetic ganglion. The dynamic gain increases in the frequency range of fc_1 to fc_2, and decreases at frequencies above fc_2.

In addition, the transfer function of the peripheral arc (SNA to systemic AP) approximates the second-order low-pass filter with a lag time in rabbits (Kamiya et al., 2005c). Therefore, the peripheral arc transfer function (H_P) can be modeled by using Equation B as follows:

$$H_P(f) = \frac{K_P}{1 + 2\zeta\frac{f}{f_N}j + \left(\frac{f}{f_N}j\right)^2} \exp(-2\pi fjL) \qquad (B)$$

where K_P is static gain (in mmHg/a.u.); f_N and ζ indicate natural frequency (in Hz) and damping ratio, respectively; and L is

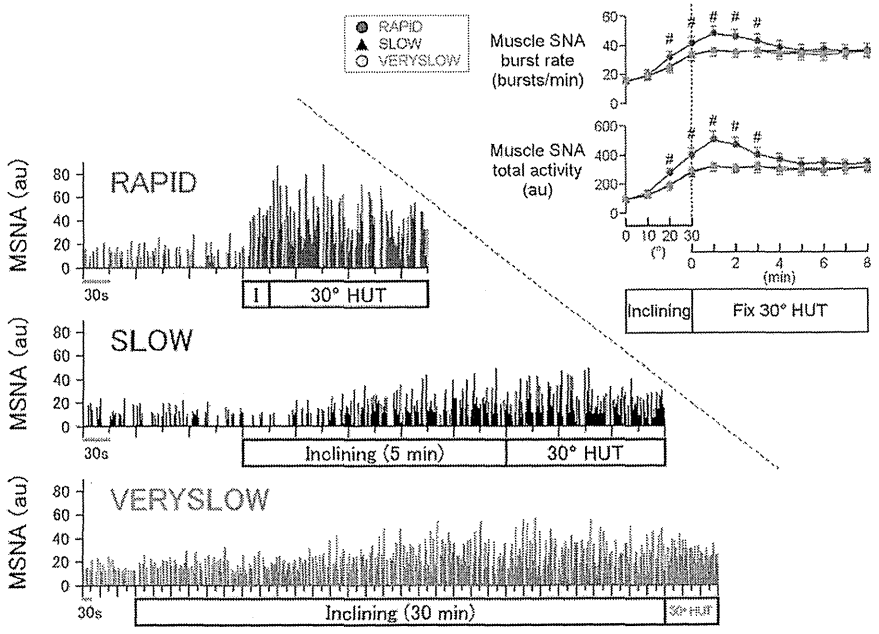

FIGURE 1 | Human MSNA responses to HUT tests with RAPID, SLOW, and VERYSLOW inclining speed. $^{\#}P < 0.05$ vs. SLOW and VERYSLOW tests. Error bars denote standard error. Modified from the study: Kamiya et al. (2009).

pure delay (in seconds), that would represent the sum of delays in the synaptic transmission at neuroeffector junction and the intracellular signal transduction in the effector organs.

NUMERICAL SIMULATION OF HUMAN MSNA RESPONSE TO HUT USING ANIMAL BAROREFLEX CHARACTERISTICS

First, a numerical simulation of the open-loop baroreflex condition was performed based on transfer functions actually identified in anesthetized animals (**Figure 2**). Since the increases in thoracic impedance averaged over tilt angle were similar in the RAPID, SLOW, and VERYSLOW HUT tests, the gravitational fluid shift directed toward the lower part of the body (such as the abdominal vascular bed and lower limbs) may be similar in all three tests at a tilt angle of 30°. Therefore, we assumed that the tilt-induced pressure perturbation was similar in the three HUT tests except for the speed. The numerical simulation indicates that in the open-loop baroreflex condition, the RAPID HUT test (1°/s) caused greater MSNA activation than SLOW (0.1°/s) and VERYSLOW (0.0167°/s) tests. This result appears to be consistent with our data observed in humans (**Figure 1**), and raises the possibility that the baroreflex control of SNA in humans also has high-pass filter characteristics.

Next, the relevance of baroreflex control of SNA to the speed-dependence in orthostatic MSNA activation was also confirmed by performing a numerical simulation mimicking the closed-loop baroreflex condition (**Figure 3**). The neural arc is arranged in series with the peripheral arc. Therefore, the total baroreflex loop is a negative-feedback control system that senses AP as baroreceptor pressure and regulates systemic AP. The simulation data indicated that the RAPID HUT test caused greater MSNA activation than the slower HUT tests, which is partially consistent with our previously observed data obtained in humans.

However, the dynamic transfer function characteristics of the neural arc cannot explain the 3-min overshoot of MSNA activation after reaching 30° HUT posture in the RAPID HUT test. In the numerical simulations, MSNA overshoot lasts less than 20 s in both baroreflex open-loop and closed-loop conditions. Accordingly, other mechanisms may be responsible for the overshoot of the orthostatic MSNA response in the faster HUT test. One possibility is a vestibulo-sympathetic response (Hammam et al., 2014; Yates et al., 2014). Another possibility is an effect of antigravity muscle contraction on SNA, since head-up suspension that removes antigravity muscle contractions caused smaller MSNA activation than HUT (Shamsuzzaman et al., 1998). Interestingly, without the numerical simulations based upon actual open-loop system identification in animals, it is difficult to predict the length of MSNA overshoot mediated by

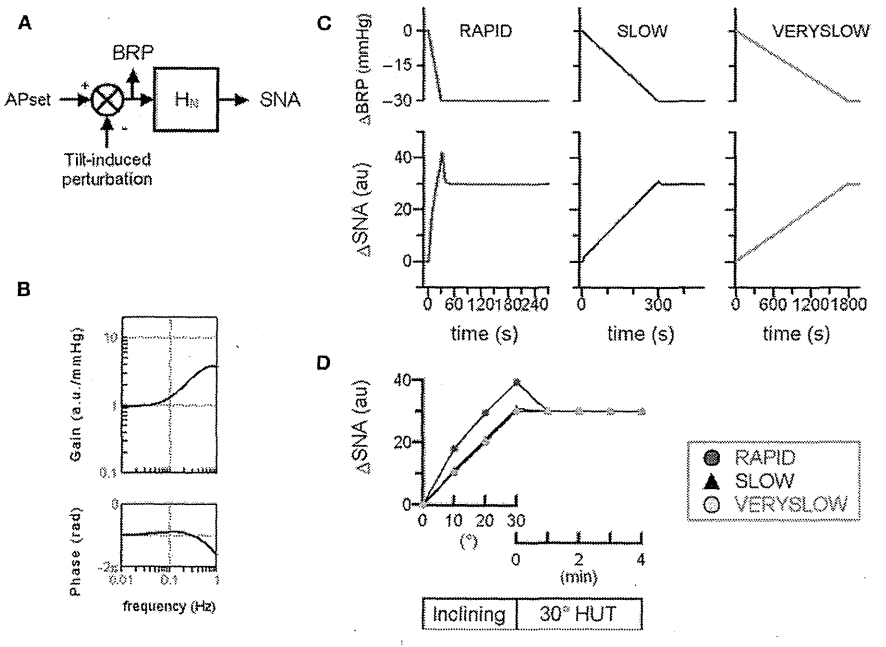

FIGURE 2 | Simulation of orthostatic activation of SNA in response to HUT at different inclining speeds in the baroreflex open-loop condition. **(A)** A block diagram of baroreflex control of SNA containing the neural arc transfer function (H_N). We assigned maximum tilt-induced perturbation of −30 mmHg in the simulations, equivalent to −1, −0.1, and −0.0167 mmHg/s in RAPID, SLOW and VERYSLOW HUT tests, respectively. We set APset at 100 mmHg. BRP; baroreceptor pressure. **(B)** The gain and phase function of H_N. The gains K_N are set at 1 au/mmHg. The fc_1, fc_2, and L are set at 0.1, 0.8, and 0.2, respectively, based on animal experimental data. **(C)** Simulated time series changes in BRP and SNA at conditions set in **(A,B)**. The RAPID test resulted in greater activation and an overshoot of SNA, compared with SLOW and VERYSLOW tests. **(D)** Simulated SNA data (same as **C**) of the RAPID (open circle), SLOW (closed triangle), and VERYSLOW (closed circle) HUT tests plotted on the same axes. Upper X-axis indicates that data are averaged over every 10° tilt angle during inclination from 0° supine to 30° HUT, while the lower X-axis indicates that data are averaged over every 1 min after reaching 30° HUT. Modified from the study: Kamiya et al. (2009).

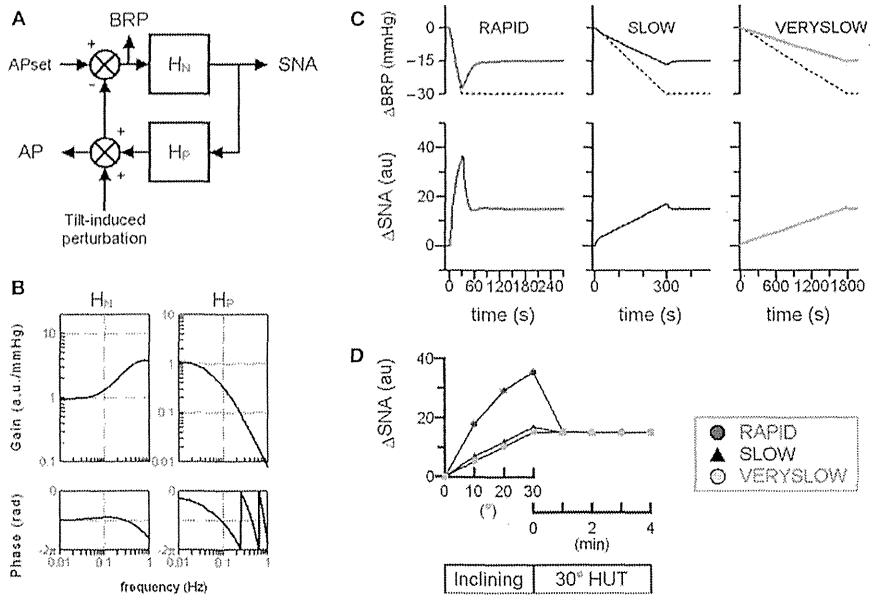

FIGURE 3 | Simulation of orthostatic activation of SNA in response to HUT at different inclining speeds in the baroreflex closed-loop condition. **(A)** A block diagram of total arc baroreflex system that contains the neural arc transfer function (H_N) and theperipheral arc transfer function (H_P). We assigned maximum tilt-induced perturbation of −30 mmHg in the simulations, equivalent to −1, −0.1, and −0.0167 mmHg/s in RAPID, SLOW and VERYSLOW HUT tests, respectively. We set APset at 100 mmHg. BRP; baroreceptor pressure. **(B)** The gain and phase function of H_N and H_P. In the model of H_N, the gain (K_N) is set at 1 au/mmHg, while the remaining parameters are set similarly in **Figure 2**. In the model of H_P, the K_P, f_N, ζ and L are set at 1, 0.07, 1.4, and 1, respectively, based on observation in animals. **(C)** Simulated time series changes in BRP (solid lines, upper panels) and SNA (lower panels) at conditions set in **(A)** and **(B)**. The dotted lines in upper panels indicate the tilt-induced perturbations. The RAPID test results in greater activation and an overshoot of SNA compared to SLOW and VERYSLOW tests. **(D)** Simulated SNA data (same as **C**) of the RAPID (open circle), SLOW (closed triangle), and VERYSLOW (closed circle) HUT tests plotted on the same axes. Upper X-axis indicates that data are averaged over every 10° tilt angle during inclination from 0° supine to 30° HUT, while the lower X-axis indicates that data are averaged over every 1 min after reaching 30° HUT.

the baroreflex and the potential involvement of mechanisms other than the baroreflex.

BAROREFLEX DYNAMIC TRANSFER CHARACTERISTICS AND BASIC CLASSIC DATA OF BARORECEPTOR AFFERENT

The baroreflex dynamic transfer function identified by a white-noise and open-loop method (Kamiya et al., 2011) is a transfer characteristics from baroreceptor pressure input to SNA in the baroreflex neural arc and that from SNA input to systemic AP in the baroreflex peripheral arc. The dynamic transfer function shows a linear component of the system, and is able to predict a time-series SNA response to randomly drug-induced (phenylephrine and nitroprusside infusions) AP changes in closed-loop condition with a high degree-of accuracy (r^2 of 0.9 ± 0.1) (Kamiya et al., 2011). However, the baroreflex dynamic transfer function is limited to address basic classic data of baroreceptor afferent, in particular the contrasting effects of static and pulsatile pressure on carotid baroreceptor activity in dogs (Chapleau and Abboud, 1987). For example, although the single unit baroreceptor afferent nerve activity increased in response to an increase in baroreceptor pressure, the pulsatile baroreceptor pressure resulted in lower threshold as compared with static (ramp-like) baroreceptor pressure. Another example is a baroreceptor afferent response to a shift from static to pulsatile pressure. A pulsatility increased afferent nerve activity at low mean arterial pressures, whereas it decreased afferent nerve activity at high mean arterial pressures. These interesting observations may relate with a non-linear component of baroreflex system.

CONCLUSION

System identification can be a powerful tool in the research of complex biosystems. However, its application for human research is often difficult since it requires open-loop surgical operation when the system is a closed-loop biosystem, which applies to the baroreflex. As a helpful challenge, I show the possibility that system identification based analysis and numerical simulation using baroreflex subsystem characteristics identified in animals can contribute to our understanding of human sympathetic physiology under orthostasis (Kamiya et al., 2005a, 2009).

REFERENCES

Chapleau, M. W., and Abboud, F. M. (1987). Contrasting effects of static and pulsatile pressure on carotid baroreceptor activity in dogs. *Circ. Res.* 61, 648–658.

Cooke, W. H., Hoag, J. B., Crossman, A. A., Kuusela, T. A., Tahvanainen, K. U., and Eckberg, D. L. (1999). Human responses to upright tilt: a window on central autonomic integration. *J. Physiol.* 517, 617–628.

Eckberg, D. L., and Sleight, P. (1992). *Human Baroreflexes in Health and Disease.* New York, NY: Oxford Univ. Press.

Fu, Q., Okazaki, K., Shibata, S., Shook, R. P., Vangunday, T. B., Galbreath, M. M., et al. (2009). Menstrual cycle effects on sympathetic neural responses to upright tilt. *J. Physiol.* 587(Pt 9), 2019–2031. doi: 10.1113/jphysiol.2008.168468

Hammam, E., Hau, C. L., Wong, K. S., Kwok, K., and Macefield, V. G. (2014). Vestibular modulation of muscle sympathetic nerve activity by the utricle during sub-perceptual sinusoidal linear acceleration in humans. *Exp. Brain Res.* 232, 1379–1388. doi: 10.1007/s00221-014-3856-6

Ikeda, Y., Kawada, T., Sugimachi, M., Kawaguchi, O., Shishido, T., Sato, T., et al. (1996). Neural arc of baroreflex optimizes dynamic pressure regulation in achieving both stability and quickness. *Am. J. Physiol.* 271, H882–H890.

Kamiya, A., Hayano, J., Kawada, T., Michikami, D., Yamamoto, K., Ariumi, H., et al. (2005a). Low-frequency oscillation of sympathetic nerve activity decreases during development of tilt-induced syncope preceding sympathetic withdrawal and bradycardia. *Am. J. Physiol. Heart Circ. Physiol.* 289, H1758–H1769.doi: 10.1152/ajpheart.01027.2004

Kamiya, A., Kawada, T., Mizuno, M., Shimizu, S., and Sugimachi, M. (2010). Parallel resetting of arterial baroreflex control of renal and cardiac sympathetic nerve activities during upright tilt in rabbits. *Am. J. Physiol. Heart Circ. Physiol.* 298, H1966–H1975. doi: 10.1152/ajpheart.00340.2009

Kamiya, A., Kawada, T., Shimizu, S., Iwase, S., Sugimachi, M., and Tadaaki Mano, T. (2009). Slow head-up tilt causes lower activation of muscle sympathetic nerve activity: loading speed-dependence of orthostatic sympathetic activation in humans. *Am. J. Physiol. Heart Circ. Physiol.* 297, H53–H58. doi: 10.1152/ajpheart.00260.2009

Kamiya, A., Kawada, T., Shimizu, S., and Sugimachi, M. (2011). Closed-loop spontaneous baroreflex transfer function is inappropriate for system identification of neural arc but partly accurate for peripheral arc: predictability analysis. *J. Physiol.* 589(Pt 7), 1769–1790. doi: 10.1152/ajpheart.00260.2009

Kamiya, A., Kawada, T., Yamamoto, K., Michikami, D., Ariumi, H., Miyamoto, T., et al. (2005c). Dynamic and static baroreflex control of muscle sympathetic nerve activity (SNA) parallels that of renal and cardiac SNA during physiological change in pressure. *Am. J. Physiol. Heart Circ. Physiol.* 289, H2641–H2648. doi: 10.1152/ajpheart.00642.2005

Kamiya, A., Kawada, T., Yamamoto, K., Michikami, D., Ariumi, H., Uemura, K., et al. (2005b). Resetting of the arterial baroreflex increases orthostatic sympathetic activation and prevents postural hypotension in rabbits. *J. Physiol.* 566(Pt 1), 237–246. doi: 10.1113/jphysiol.2005.086512

Kamiya, A., Kawada, T., Yamamoto, K., Mizuno, M., Shimizu, S., and Sugimachi, M. (2008). Upright tilt resets dynamic transfer function of baroreflex neural arc to minify the pressure disturbance in total baroreflex control. *J. Physiol. Sci.* 58, 189–198. doi: 10.2170/physiolsci.RP004308

Kawada, T., Zheng, C., Yanagiya, Y., Uemura, K., Miyamoto, T., Inagaki, M., et al. (2002). High-cut characteristics of the baroreflex neural arc preserve baroreflex gain against pulsatile pressure. *Am. J. Physiol. Heart Circ. Physiol.* 282, H1149–H1156. 10.1152/ajpheart.00750.2001

Shamsuzzaman, A. S., Sugiyama, Y., Kamiya, A., Fu, Q., and Mano, T. (1998). Head-up suspension in humans: effects on sympathetic vasomotor activity and cardiovascular responses. *J. Appl. Physiol.* 84, 1513–1519.

Yates, B. J., Bolton, P. S., and Macefield, V. G. (2014). Vestibulo-sympathetic responses. *Compr. Physiol.* 4, 851–887. doi: 10.1002/cphy.c130041

Conflict of Interest Statement: The authors declare that the research was conducted in the absence of any commercial or financial relationships that could be construed as a potential conflict of interest.

Received: 17 April 2014; accepted: 17 June 2014; published online: 08 July 2014.
Citation: Kamiya A, Kawada T and Sugimachi M (2014) Systems physiology of the baroreflex during orthostatic stress: from animals to humans. Front. Physiol. 5:256. doi: 10.3389/fphys.2014.00256
This article was submitted to Integrative Physiology, a section of the journal Frontiers in Physiology.

Circulation Journal
Official Journal of the Japanese Circulation Society
http://www.j-circ.or.jp

ORIGINAL ARTICLE
Heart Failure

Medetomidine Suppresses Cardiac and Gastric Sympathetic Nerve Activities but Selectively Activates Cardiac Vagus Nerve

Shuji Shimizu, MD, PhD; Tsuyoshi Akiyama, MD, PhD; Toru Kawada, MD, PhD; Atsunori Kamiya, MD, PhD; Michael James Turner, PhD; Hiromi Yamamoto, MD, PhD; Toshiaki Shishido, MD, PhD; Mikiyasu Shirai, MD, PhD; Masaru Sugimachi, MD, PhD

Background: To identify a pharmacological agent that can selectively activate cardiac vagus nerve for potential use in vagal activation therapy against heart failure, the effects of medetomidine on autonomic nerve activities in both the heart and stomach were examined.

Methods and Results: In anesthetized rabbits, microdialysis probes were implanted into both the right atrial and gastric walls. Dialysate acetylcholine (ACh) and norepinephrine (NE) concentrations were measured by high-performance liquid chromatography. First, the effects of 100 μg/kg of intravenous medetomidine on vagal ACh and sympathetic NE releases were examined. Medetomidine significantly increased cardiac ACh release (4.7±1.1 to 7.8±0.9 nmol/L, P<0.05), but suppressed gastric ACh release (8.0±2.6 to 3.5±1.5 nmol/L, P<0.01). In contrast, medetomidine suppressed both cardiac and gastric NE releases. Second, the effects of medetomidine on ACh releases induced by electrical vagus nerve stimulation (VNS; 10 Hz) were examined. Electrical VNS significantly increased both cardiac (6.7±1.2 to 14.8±1.8 nmol/L, P<0.01) and gastric (3.8±0.8 to 181.3±65.6 nmol/L, P<0.01) ACh releases. Medetomidine did not alter the VNS-induced increases in ACh release.

Conclusions: Medetomidine suppresses both cardiac and gastric sympathetic nerve activities. In contrast, medetomidine activates cardiac vagus nerve but inhibits gastric vagal activity. Medetomidine might be one of the potential pharmacological agents for vagal activation therapy against heart failure without the risk of gastric adverse effects. (*Circ J* 2014; **78:** 1405–1413)

Key Words: Acetylcholine; α2-adrenergic agonist; Norepinephrine; Sympathetic nerve activity; Vagus nerve activity

Electrical vagus nerve stimulation (VNS) has remained a therapeutic option for epileptic seizures for several decades. Recently, electrical VNS has also been evaluated as a direct method to correct autonomic imbalance (activated sympathetic nerve system and suppressed vagus nerve activity) in patients with chronic heart failure (CHF).[1] The effect of VNS in CHF patients is being studied in an on-going multicenter international clinical trial, the INcrease Of VAgal TonE in Heart Failure study (INOVATE-HF).[2] However, from the clinical experience of using electrical VNS in patients with epileptic seizures, electrical stimulation of the cervical vagus nerve might cause several gastrointestinal adverse effects such as nausea and diarrhea.[3,4]

To avoid these adverse effects, selective activation of cardiac vagus nerve might be favorable. We have reported that a selective α2-adrenergic agonist, medetomidine (a racemic mixture of dexmedetomidine and levomedetomidine), suppresses sympathetic norepinephrine (NE) release and enhances vagal acetylcholine (ACh) release to the sinoatrial node.[5] In contrast, dexmedetomidine has been reported to have an antiulcerative effect on indomethacin-induced gastric ulcers,[6] suggesting that medetomidine or dexmedetomidine might be able to activate cardiac vagus nerve without undesirable gastrointestinal effects. Thus, medetomidine might be one of the potential pharmacological agents for vagal activation therapy against CHF.

We have established a microdialysis technique for in vivo monitoring of neuronal NE and ACh releases to the rabbit sinoatrial node.[7,8] Local sampling of the microdialysis technique

Received November 28, 2013; revised manuscript received March 4, 2014; accepted March 6, 2014; released online April 11, 2014 Time for primary review: 13 days

Department of Cardiovascular Dynamics (S.S., T.K., A.K., M.J.T., T.S., M. Sugimachi), Department of Cardiac Physiology (T.A., M. Shirai), National Cerebral and Cardiovascular Center, Suita; and Division of Cardiology, Department of Medicine, Faculty of Medicine, Kinki University, Osaka-sayama (H.Y.), Japan

Mailing address: Shuji Shimizu, MD, PhD, Department of Cardiovascular Dynamics, National Cerebral and Cardiovascular Center, 5-7-1 Fujishiro-dai, Suita 565-8565, Japan. E-mail: shujismz@ri.ncvc.go.jp

ISSN-1346-9843 doi:10.1253/circj.CJ-13-1456

Table. Doses of Intravenous Phenylephrine Infusion Used to Maintain Mean Arterial Pressure at Baseline Level

(n=6)	Baseline after vagotomy	Bil. VNS	Medetomidine + Bil. VNS	Medetomidine + Bil. VNS + C6
Phenylephrine ($\mu g \cdot kg^{-1} \cdot min^{-1}$)	0	13.1±1.6	9.1±1.8	9.0±2.5

Bil. VNS, bilateral vagus nerve stimulation; C6, hexamethonium.

allows monitoring of ACh and NE releases as indices of organ-specific autonomic nerve activities. In the present study, we applied the microdialysis technique to both the heart and stomach of rabbits and examined the effects of medetomidine on organ-specific autonomic nerve activities.

Methods

Surgical Preparation

Animal care was provided in accordance with the *Guiding Principles for the Care and Use of Animals in the Field of Physiological Sciences* published by the Physiological Society of Japan. All protocols were approved by the Animal Subject Committee of the National Cerebral and Cardiovascular Center. Twenty-four Japanese white rabbits weighing 2.5–3.2 kg were used in this study. Anesthesia was initiated by an intravenous injection of pentobarbital sodium (50 mg/kg) via the marginal ear vein, and then maintained at an appropriate level by continuous intravenous infusion of α-chloralose and urethane ($16 mg \cdot kg^{-1} \cdot h^{-1}$ and $100 mg \cdot kg^{-1} \cdot h^{-1}$, respectively). An adequate anesthesia level was confirmed by loss of the ear pinch response. The animals were intubated and ventilated mechanically with room air mixed with oxygen. The respiratory rate and tidal volume were set at 30 cycles/min and 15 ml/kg, respectively. Systemic arterial pressure was monitored by a catheter inserted into the femoral artery. Heparin sodium ($10 IU \cdot kg^{-1} \cdot h^{-1}$) was infused to prevent blood coagulation in the femoral artery catheter. Esophageal temperature was maintained between 38 and 39°C using a heating pad.

With the animal in the supine position, a right lateral thoracotomy was performed and the right 3rd to 5th ribs were partially resected to expose the heart. After incision of the pericardium, a dialysis probe was implanted into the atrial wall near the sinoatrial node, as described in the *Dialysis Technique* section below. A midline laparotomy was also performed to expose the stomach. Another dialysis probe was implanted into the anterior wall of the stomach as described in the *Dialysis Technique* section.

Three stainless steel electrodes were attached around the thoracotomy incision for recording body surface electrocardiogram. The heart rate was determined from the electrocardiogram or arterial pressure waveform using a cardiotachometer.

At the end of the experiment, the animal was euthanized by injecting an overdose of pentobarbital sodium. In a post-mortem examination, the right atrial wall and the anterior wall of the stomach were resected en bloc with the dialysis probes. The internal surfaces of the atrial and gastric walls were examined macroscopically to confirm that the dialysis membranes were not exposed to the right atrial lumen and the gastric cavity.

Dialysis Technique

The materials and properties of the dialysis probe have been described previously.[7–10] A dialysis fiber of a semipermeable membrane (length 4 mm, outer diameter 310 μm, inner diameter 200 μm, PAN-1200, molecular weight cut-off 50,000; Asahi Chemical, Tokyo, Japan) was attached at both ends to polyethylene tubes. One dialysis probe was implanted into the right atrial myocardium near the sinoatrial node, which has the richest vagal innervation in the heart.[11] Another dialysis probe was implanted into the anterior wall of the stomach because peristaltic movement was relatively smaller than the other part of the gastrointestinal tract. After implantation, these dialysis probes were perfused with Ringer's solution (NaCl 147 mmol/L, KCl 4 mmol/L, $CaCl_2$ 3 mmol/L) alone for NE measurement, or with Ringer's solution containing a cholinesterase inhibitor, eserine (100 μmol/L), for ACh measurement, at a speed of 2 μl/min using a microinjection pump (CMA/102; Carnegie Medicin, Stockholm, Sweden). Experimental protocols were started 2 h after implantation of the dialysis probes. The dead space between the dialysis membrane and the sample tube was taken into account at the beginning of each dialysate sampling. Four microliters of phosphate buffer (pH 3.5) was added to each sample tube before dialysate sampling, and each dialysate sampling period was set at 10 min (1 sample volume=20 μl). In the supplementary protocol, 8-μl of phosphate buffer was added to each sample tube, and each dialysate sampling period was set at 20 min (1 sample volume=40 μl). The dialysate ACh or NE concentration was analyzed by high-performance liquid chromatography, as described previously.[9,10]

Experimental Protocols

Protocol 1 (n=13) We investigated the effects of intravenous medetomidine on both cardiac and gastric vagal ACh (n=7) and sympathetic NE (n=6) releases. First, 10-min baseline dialysate samples were collected under baseline conditions. Thereafter, 100 μg/kg of medetomidine, which has been shown to increase the cardiac dialysate ACh concentration,[5] was injected intravenously via the femoral vein. After hemodynamic stabilization, dialysate samples were collected for 10 min (20 μl). Immediately after the second sampling, intravenous infusion of phenylephrine was started ($4.3 \pm 0.7 \mu g \cdot kg^{-1} \cdot min^{-1}$) to restore mean arterial pressure to the baseline level because a decrease in mean arterial pressure during the second sampling might have affected sympathetic and vagal outflows through the arterial baroreflex. After hemodynamic stabilization, dialysate samples were again collected for 10 min.

Protocol 2 (n=6) We investigated the effect of medetomidine on both cardiac and gastric ACh releases induced by electrical stimulation of bilateral cervical vagus nerves. Because there was a difference in vagal innervations between the right atrium and anterior wall of the stomach, bilateral vagus nerves were exposed through a midline cervical incision and sectioned at the neck region to perform a simultaneous stimulation to both the heart and stomach. A pair of bipolar stainless steel electrodes was attached to the efferent side of each vagus nerve. The nerves and electrodes were immobilized using a quick-curing silicone gel (Kwik-Sil; World Precision Instruments, Inc, FL, USA). After sampling the baseline dialysates, bilateral efferent vagus nerves were simultaneously stimulated at a frequency of 10 Hz using a digital stimulator (SEN-7203; Nihon Kohden, Japan). The pulse duration and amplitude of nerve stimulation were set at 1 ms and 10 V, respectively. To main-

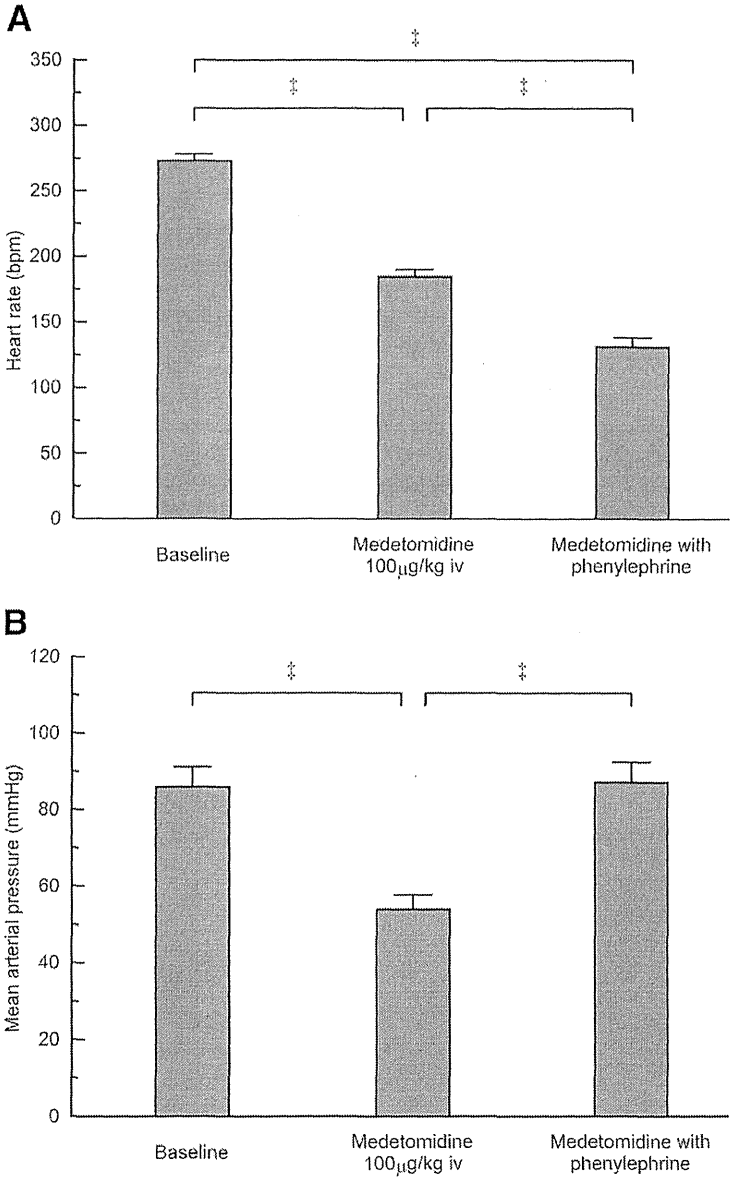

Figure 1. Effects of 100 μg/kg of medetomidine on heart rate (**A**) and mean arterial pressure (**B**) (n=13). All data are presented as mean±SE. iv, intravenous injection. ‡P<0.01.

tain mean arterial pressure at the baseline level, intravenous infusion of phenylephrine was started simultaneously to VNS (**Table**), and dialysates were sampled for 10 min (20 μl). Thereafter, to examine the effect of medetomidine on electrical VNS-induced ACh releases from nerve endings, 100 μg/kg of medetomidine was injected intravenously via the femoral vein. After hemodynamic stabilization, dialysate samples were again collected for 10 min under 10-Hz electrical VNS. Finally, a ganglionic blocker, hexamethonium bromide (30 mg/kg), was injected intravenously and 10-min dialysate samples were collected under 10-Hz VNS.

Supplementary protocol (n=5) We investigated the effects of intravenous atipamezole, an α_2-adrenergic antagonist, on both medetomidine-induced cardiac and gastric vagal ACh and sympathetic NE responses. First, 20-min baseline dialysate samples were collected under baseline conditions. Thereafter, 100 μg/kg of medetomidine was injected intravenously via the femoral vein. After hemodynamic stabilization, dialysate samples were collected for 20 min (40 μl). Immediately after the second sampling, 2.5 mg/kg of atipamezole was injected intravenously. After hemodynamic stabilization, dialysate samples were again collected for 20 min.

Statistical Analysis

All data are presented as mean±standard error. Heart rate and mean arterial pressure were compared by using one-way repeated measures analysis of variance (ANOVA) followed by a Holm's test.[12] After logarithmic transformation, dialysate ACh and NE concentrations were also compared by using one-way repeated measures ANOVA followed by a Holm's test. In the supplementary protocol, after logarithmic transformation, dialysate ACh and NE concentrations were compared by using one-way repeated measures ANOVA followed by a Dunnett's test against baseline values. Differences were con-

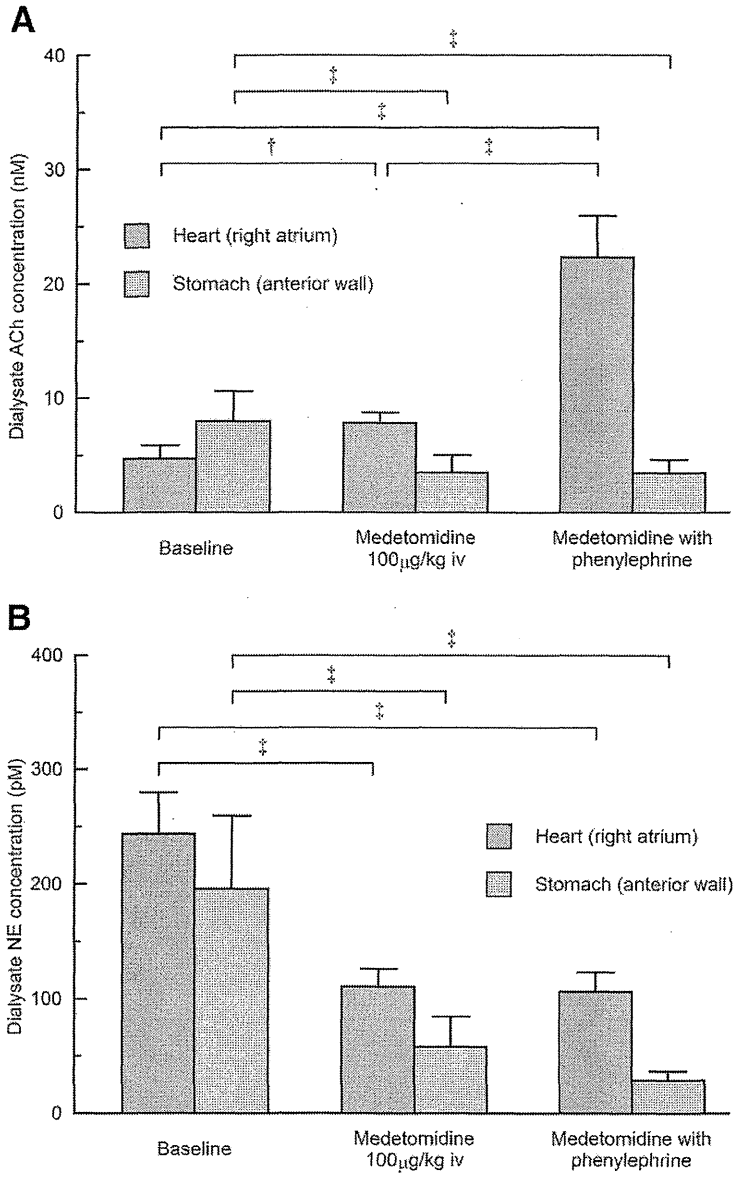

Figure 2. Effects of 100 μg/kg of medetomidine on dialysate acetylcholine (**A**, n=7) and norepinephrine (**B**, n=6) concentrations. All data are presented as mean±SE. ACh, acetylcholine; NE, norepinephrine; iv, intravenous injection. †P<0.05; ‡P<0.01.

sidered significant at P<0.05.

Results

Protocol 1

An intravenous injection of 100 μg/kg of medetomidine significantly decreased the heart rate from 273±5bpm at baseline to 185±6bpm (P<0.01) (**Figure 1A**), and the mean arterial pressure from 87±3 mmHg to 52±2 mmHg (P<0.01) (**Figure 1B**). This dose of medetomidine significantly increased the cardiac dialysate ACh concentration from 4.7±1.1 nmol/L at baseline to 7.8±0.9 nmol/L (P<0.05), but decreased the gastric dialysate ACh concentration from 8.0±2.6 nmol/L at baseline to 3.5±1.5 nmol/L (P<0.01) (**Figure 2A**). The medetomidine injection significantly decreased the cardiac dialysate NE concentration from 244±36 pmol/L at baseline to 111±16 pmol/L (P<0.01) and also the gastric dialysate NE concentration from 196±64 pmol/L at baseline to 58±27 pmol/L (P<0.01) (**Figure 2B**).

After the medetomidine injection and dialysate sampling, infusion of phenylephrine restored the mean arterial pressure to the baseline level (90±3 mmHg, not significant vs. baseline) and decreased the heart rate significantly (132±7 bpm, P<0.01 vs. medetomidine alone) (**Figures 1A,B**). After the medetomidine injection, infusion of phenylephrine increased the cardiac dialysate ACh concentration to a significantly higher level than that of medetomidine alone (22.3±3.6 nmol/L, P<0.01), but it did not change the gastric dialysate ACh concentration (3.5±1.1 nmol/L, not significant vs. medetomidine alone) (**Figure 2A**). Infusion of phenylephrine subsequent to the medetomidine injection did not change the cardiac or gastric dialysate NE concentration (not significant vs. medetomidine alone), and both cardiac (106±17 pmol/L, P<0.01 vs. baseline) and gastric dialysate NE concentrations (29±8 pmol/L, P<0.01

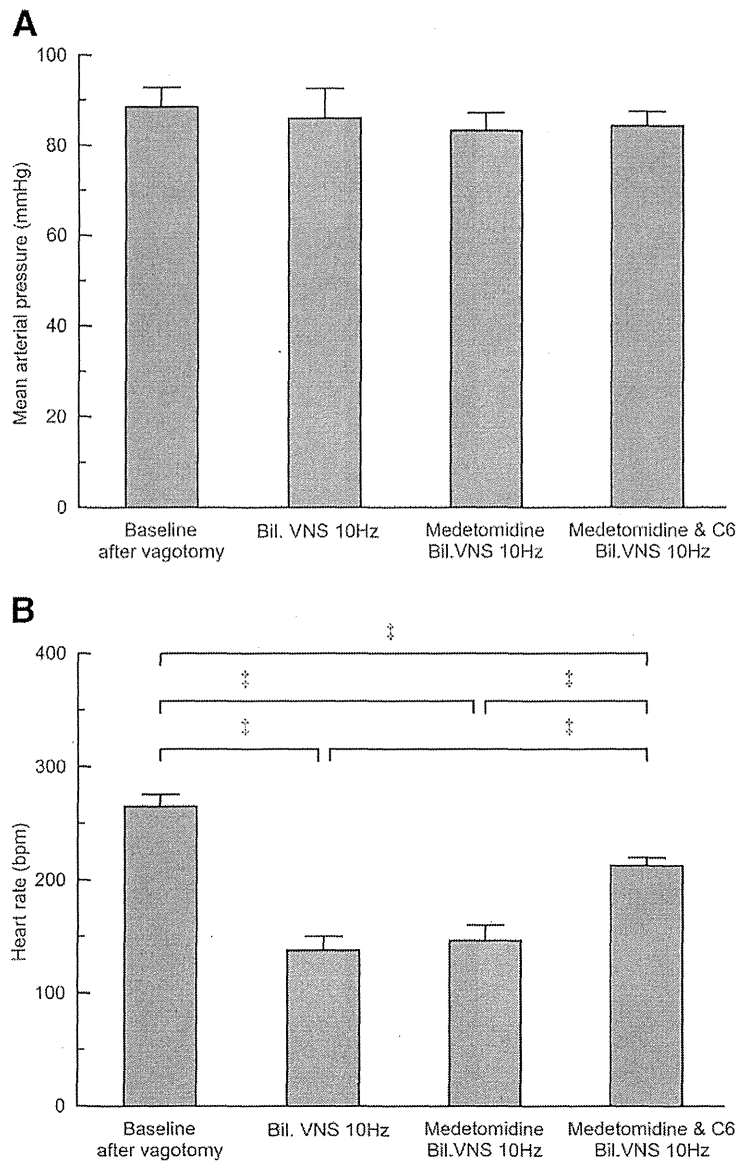

Figure 3. Effects of medetomidine injection on mean arterial pressure (**A**) and heart rate (**B**) in rabbits undergoing bilateral electrical vagus nerve stimulation (10Hz, 1ms, 10V) and intravenous infusion of phenylephrine (n=6). All data are presented as mean±SE. Bil., bilateral; VNS, vagus nerve stimulation; C6, hexamethonium. ‡P<0.01.

vs. baseline) remained significantly reduced compared to baseline levels (**Figure 2B**).

Protocol 2

The mean arterial pressure was maintained at the same level as that of the baseline by intravenous infusion of phenylephrine during VNS throughout the experiment (**Figure 3A**). Bilateral electrical VNS at a frequency of 10Hz significantly decreased the heart rate from 265±10bpm at baseline to 138±12bpm (P<0.01) (**Figure 3B**). The 10-Hz VNS significantly increased the cardiac dialysate ACh concentration from 6.7±1.2nmol/L at baseline to 14.8±1.8nmol/L (P<0.01) (**Figure 4A**) and the gastric dialysate ACh concentration from 3.8±0.8nmol/L at baseline to 181.3±65.6nmol/L (P<0.01) (**Figure 4B**). Under a 10-Hz electrical VNS, injection of 100-μg/kg medetomidine did not alter the heart rate (146±14bpm) (**Figure 3B**), and it did not affect the cardiac (13.6±2.2nmol/L) or gastric (196.7±70.7nmol/L) dialysate ACh concentration (**Figures 4A,B**).

Subsequent to the medetomidine injection under a 10-Hz vagal stimulation, an intravenous injection of 30mg/kg hexamethonium bromide significantly reduced both the cardiac and gastric dialysate ACh concentrations (7.2±1.5nmol/L and 9.7±2.7nmol/L, respectively) (**Figures 4A,B**). However, the gastric dialysate ACh concentration remained higher than that of the baseline level (P<0.01 vs. baseline).

Supplementary Protocol

An intravenous injection of 100μg/kg of medetomidine significantly increased the cardiac dialysate ACh concentration from 5.2±1.1nmol/L at baseline to 8.4±1.4nmol/L (P<0.01), but decreased the gastric dialysate ACh concentration from 6.4±1.8nmol/L at baseline to 3.6±1.0nmol/L (P<0.01) (**Figure 5A**). The medetomidine injection signifi-

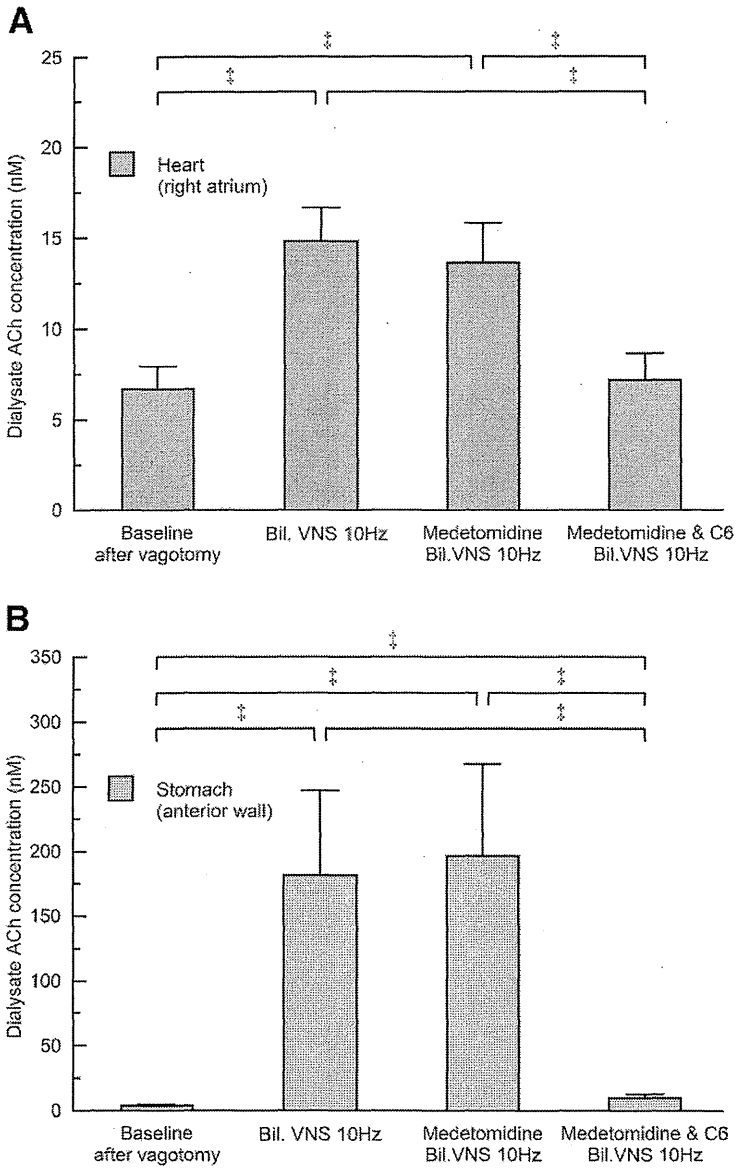

Figure 4. Effects of medetomidine injection on cardiac (**A**) and gastric (**B**) dialysate acetylcholine concentrations in rabbits undergoing bilateral electrical vagus nerve stimulation (10Hz, 1ms, 10V) and intravenous infusion of phenylephrine. All data are presented as mean ±SE. ACh, acetylcholine; Bil., bilateral; VNS, vagus nerve stimulation; C6, hexamethonium. ‡P<0.01.

cantly decreased the cardiac dialysate NE concentration from 472±88pmol/L at baseline to 266±47pmol/L (P<0.05) and also the gastric dialysate NE concentration from 381±116pmol/L at baseline to 130±29pmol/L (P<0.05) (**Figure 5B**). An intravenous injection of 2.5mg/kg of atipamezole restored both the cardiac and gastric dialysate ACh concentrations to the baseline levels (6.0±1.2 and 7.6±2.6nmol/L, respectively) (**Figure 5A**). Atipamezole also restored both the cardiac and gastric dialysate NE concentrations to the baseline levels (436±102 and 385±130pmol/L, respectively) (**Figure 5B**).

Discussion

Simultaneous monitoring of both the cardiac and gastric vagal ACh and sympathetic NE releases demonstrated that medetomidine enhanced cardiac ACh release but suppressed gastric ACh release to the stomach. In contrast, medetomidine suppressed both the cardiac and gastric NE releases.

Effects of Medetomidine on Vagal ACh Releases

The present study demonstrated that electrical stimulation of bilateral cervical vagus nerves at a frequency of 10Hz significantly increased both the cardiac and gastric ACh releases. This result suggests that electrical stimulation of cervical vagus nerves might activate the whole vagal system. However, the extent of vagal activation might differ in various organs. Although baseline dialysate ACh concentrations in the heart and in the stomach did not differ (6.7±1.2nmol/L and 3.8±0.8nmol/L, respectively; not significant as found by an unpaired t-test), the dialysate ACh concentration during 10-Hz VNS was 12-times higher in the stomach (181.3±65.6nmol/L) than that in the heart (14.8±1.8nmol/L) (P<0.01 by an unpaired t-test). This difference in magnitude of a dialysate ACh response might reflect a difference in density of vagal innervation between the heart

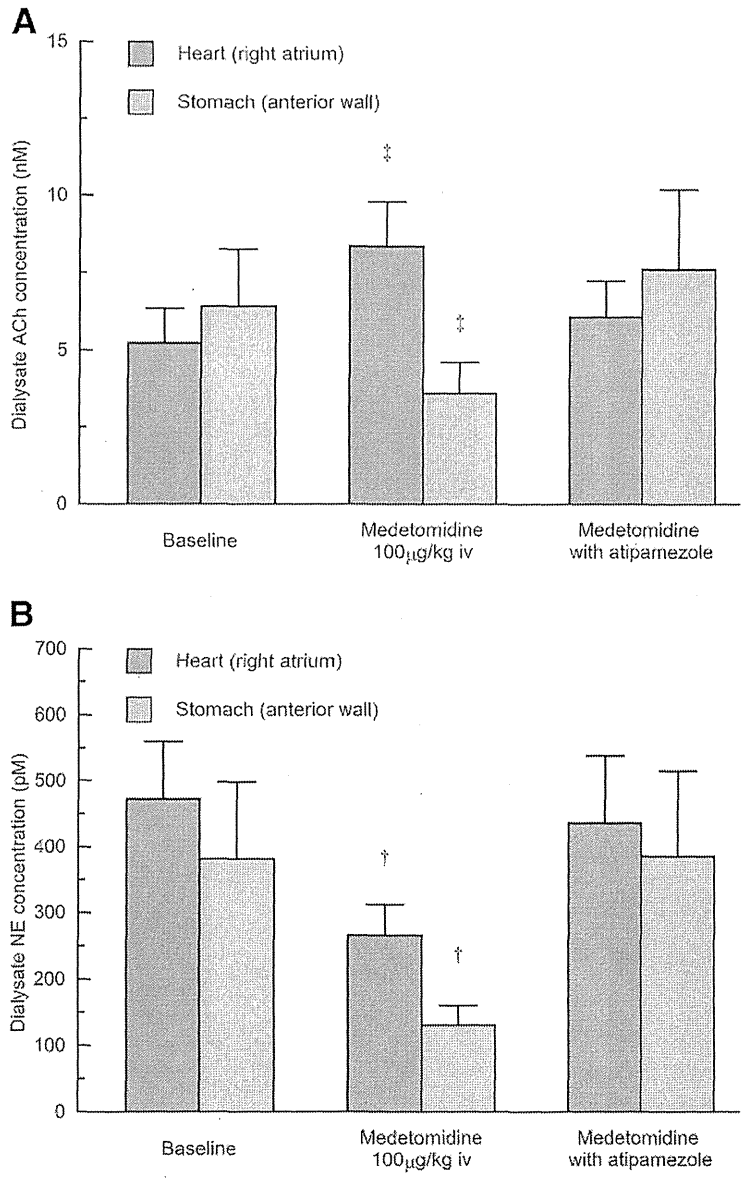

Figure 5. Effects of 2.5 mg/kg of atipamezole on medetomidine-induced acetylcholine (**A**) and norepinephrine (**B**) responses. All data are presented as mean±SE. ACh, acetylcholine; NE, norepinephrine; iv, intravenous injection. †P<0.05; ‡P<0.01.

and the stomach. In clinical settings, although weaker electrical VNS at a lower frequency and lower voltage compared to the present study is used, electrical VNS might cause unexpected vagal activation in non-target organs, resulting in adverse effects.

In contrast to electrical VNS, vagal response to medetomidine differs in the heart and in the stomach. In protocol 1, 100 μg/kg of medetomidine significantly increased the cardiac ACh release but suppressed the gastric ACh release. As shown in protocol 2, medetomidine scarcely affected VNS-induced cardiac and gastric ACh releases, suggesting that the effects of medetomidine on vagus ganglion and postganglionic vagus nerve terminals were small. Furthermore, hexamethonium, which blocks ganglionic transmission between preganglionic and postganglionic neurons, almost completely suppressed the VNS-induced ACh releases. This finding suggests that dialysate ACh concentration monitored by microdialysis mainly reflects ACh release from postganglionic vagus nerve endings, and the peripheral effects of medetomidine on nerve endings should be small. Furthermore, the supplementary protocol demonstrated that medetomidine-induced vagal ACh responses in both the heart and stomach were almost completely diminished by an α_2-adrenergic antagonist, atipamezole. Therefore, we think that medetomidine-induced vagal activation mainly depends on its central α_2-adrenergic action.

In protocol 1, restoring the mean arterial pressure to baseline level using phenylephrine enhanced medetomidine-induced cardiac ACh release. As we have already demonstrated that medetomidine enhances cardiac ACh release through modulation of the baroreflex control,[5] this vagotonic effect of medetomidine on the heart should be dependent on the baroreflex response. Robertson and Leslie showed that α_2-adrenergic receptors are densely distributed in the nucleus tractus solitaries (NTS), where baroreceptor afferent nerves terminate.[13] Grutu et al.